

Article

# Effects of Decaphenylcyclopentasilane Addition on Photovoltaic Properties of Perovskite Solar Cells

Masaya Taguchi <sup>1</sup>, Atsushi Suzuki <sup>1</sup> , Takeo Oku <sup>1,\*</sup> , Sakiko Fukunishi <sup>2</sup>, Satoshi Minami <sup>2</sup> and Masanobu Okita <sup>2</sup>

<sup>1</sup> Department of Materials Science, The University of Shiga Prefecture, 2500 Hassaka, Hikone, Shiga 522-8533, Japan; of21mtaguchi@ec.usp.ac.jp (M.T.); suzuki@mat.usp.ac.jp (A.S.)

<sup>2</sup> Frontier Materials Laboratories, Osaka Gas Chemicals Co., Ltd., Osaka 554-0051, Japan; fukunishi@ogc.co.jp (S.F.); s-minami@ogc.co.jp (S.M.); okita@ogc.co.jp (M.O.)

\* Correspondence: oku@mat.usp.ac.jp; Tel.: +81-749-28-8368; Fax: +81-749-28-8590

Received: 8 November 2018; Accepted: 10 December 2018; Published: 13 December 2018



**Abstract:** Perovskite solar cells, in which decaphenylcyclopentasilane (DPPS) layers were formed on the surface of the perovskite layer, were fabricated, and the influence on photovoltaic characteristics was investigated. The devices were fabricated by a spin-coating technique, and the surface morphology and crystal structures were investigated by scanning electron microscopy and X-ray diffraction. By adding the DPPS, the fill factor and open circuit voltage were increased, and the photoelectric conversion efficiency was improved. A stability test in ambient air was carried out for seven weeks, and the photoelectric conversion efficiencies were remarkably improved for the devices with DPPS.

**Keywords:** perovskite solar cells; polysilane derivative; stability

## 1. Introduction

The organic–inorganic metal halide perovskite-type solar cells (PSCs) are the most promising devices for renewable energy because they have characteristics of high optical absorption coefficient, long exciton diffusion length, and high carrier mobility [1–6]. In recent years, the photoelectric conversion efficiencies of the perovskite solar cells have reached more than 20% [7–10]. However, perovskite solar cells have several problems, including stability, reproducibility, and abnormal hysteresis [11,12]. In order to solve such problems, researches and developments of perovskite solar cells using polymeric materials have been conducted [13–18]. Although 2,2',7,7'-tetrakis-(*N,N*-di(*p*-methoxyphenyl)amine)-9,9'-spirobifluorene (spiro-OMeTAD) are quite often used as a hole transport layer (HTL) for the perovskite cells, there are problems in the cost and stability. Alternative hole transport materials and improvement of the stability have also been reported [19–23]. Recently, many researches on perovskite solar cells using poly(methyl methacrylate) (PMMA) have been reported [24–27]. By depositing the PMMA layer on the perovskite layer, the PMMA forms a compact layer based on the cross-linking network and protects the device from oxygen and moisture [28]. However, since PMMA is an insulating material, accurate control of film thickness is mandatory. If even just a little thick film is formed, the resistance value increases and the conversion efficiency decreases [27]. Other polymer materials, including polysilane derivatives, have been applied to organic solar cells [29–31]. The polysilanes were also applied as a hole transport layer for perovskite solar cells [32,33], and the photovoltaic performance was improved for a device using decaphenylcyclopentasilane (DPPS). However, there are few reports on the application of the polysilane derivatives to the perovskite photoactive layers [34], except for the hole transport layers [32].

The purpose of the work presented was to investigate photovoltaic properties of CH<sub>3</sub>NH<sub>3</sub>PbI<sub>3</sub> (MAPbI<sub>3</sub>) perovskite-type solar cells with DPPS prepared by a simple spin-coating technique in ambient

air. There are two advantages for the DPPS. The first is that the DPPS is a p-type semiconductor, and this facilitates hole transfer and rectification at the *pn* junction. The second is that the DPPS has high stability and acts as a protective layer on the photoactive layer. In previous research, DPPS has been used for the HTLs or additives to the perovskite precursor solutions. Here, the DPPS layer was formed on the perovskite layer during spin-coating of the perovskite layer, which enabled formation of an intermediate layer between the spiro-OMeTAD HTL and the photoactive perovskite layer. The effects of DPPS addition on the top of perovskite layer on the photovoltaic properties and microstructures were investigated using light-induced current density voltage (*J*–*V*) characteristics, external quantum efficiency (EQE) measurements, XRD, optical microscopy (OM), and SEM.

## 2. Materials and Methods

A schematic illustration of the fabrication process of the proposed MAPbI<sub>3</sub>/(DPPS) (*X* mg mL<sup>−1</sup>) photovoltaic cells is shown in Figure 1. The detailed fabrication process was described in previous reports [35–37]. Each layer was formed by the spin-coating method. F-doped tin oxide (FTO) substrates were cleaned using an ultrasonic bath with acetone and methanol and dried under nitrogen gas. Precursor solutions of 0.15 and 0.30 M TiO<sub>2</sub>, respectively, were prepared from titanium diisopropoxide bis (acetyl acetonate) (0.055 and 0.11 mL, Sigma Aldrich, Tokyo, Japan) with 1-butanol (1 mL, Nacalai Tesque, Kyoto, Japan). The 0.15 M TiO<sub>2</sub> precursor solution was spin-coated on the FTO substrate at 3000 rpm for 30 s and annealed at 125 °C for 5 min. This process of 0.30 M solution was performed twice, and the FTO substrate was sintered at 550 °C for 30 min to form a compact TiO<sub>2</sub> layer. For the mesoporous TiO<sub>2</sub> layer, the TiO<sub>2</sub> paste was prepared with TiO<sub>2</sub> powder (P-25, Aerosil, Tokyo, Japan) with poly(ethylene glycol) (PEG #20000, Nacalai Tesque, Kyoto, Japan) in ultrapure water [38]. The solution was mixed with acetylacetone (10 μL, Fujifilm Wako Pure Chemical Corporation, Osaka, Japan) and triton X-100 (5 μL, Sigma Aldrich, Tokyo, Japan) for 30 min, and left for 24 h to suppress bubbles in the solution. After that, TiO<sub>2</sub> paste was coated on the substrate by spin-coating at 5000 rpm for 30 s. The cells were annealed at 125 °C for 5 min and sintered at 550 °C for 30 min to form the mesoporous TiO<sub>2</sub> layer [39]. For preparation of the perovskite compounds, solutions of CH<sub>3</sub>NH<sub>3</sub>I (190.7 mg, Tokyo Chemical Industry, Tokyo, Japan), PbCl<sub>2</sub> (111.2 mg, Sigma Aldrich, Tokyo, Japan) with the desired molar ratio in *N,N*-dimethylformamide (0.5 mL, Sigma Aldrich, Tokyo, Japan), was mixed at 60 °C for 24 h. The perovskite precursor solutions were normally spin-coated during the first experiments. During the second and third experiments, an air flow method was applied and spin-coating at 2000 rpm for 60 s was carried out [40]. The standard cells were annealed at 140 °C, and the cells with added DPPS were annealed at 160 °C for 10 min (when the starting materials are CH<sub>3</sub>NH<sub>3</sub>I + PbI<sub>2</sub>, the 100 °C annealing is better, which was also confirmed in the previous works [34,35]; here, the starting materials are 3CH<sub>3</sub>NH<sub>3</sub>I + PbCl<sub>2</sub>, and CH<sub>3</sub>NH<sub>3</sub>PbI<sub>3</sub> + 2CH<sub>3</sub>NH<sub>3</sub>Cl(gas) were formed after the reaction at 140 °C [41]). DPPS (Osaka Gas Chemicals, Osaka, Japan) solutions with different DPPS concentrations were prepared using chlorobenzene (0.5 mL, Fujifilm Wako Pure Chemical Corporation, Osaka, Japan). The concentration of DPPS was adjusted to *X* = 0–20 mg mL<sup>−1</sup>. The DPPS solution was dropped onto the perovskite layer during the last 15 s of spin-coating of the perovskite precursor solutions. Then, a HTL was prepared by spin-coating at 4000 rpm for 30 s. For the HTL, a solution of 2,2',7,7'-tetrakis(*N,N*-di(*p*-methoxyphenyl)amine)-9,9'-spirobifluorene (36.1 mg, Spiro-OMeTAD, Sigma Aldrich, Tokyo, Japan) in chlorobenzene (0.5 mL, Fujifilm Wako Pure Chemical Corporation, Osaka, Japan) was mixed with a solution of lithium bis (trifluoromethylsulfonyl) imide (260 mg, Li-TFSI, Tokyo Chemical Industry, Tokyo, Japan) in acetonitrile (0.5 mL, Sigma Aldrich, Tokyo, Japan) for 24 h. The former solution with 4-tertbutylpyridine (14.4 μL, Sigma Aldrich, Tokyo, Japan) was mixed with the Li-TFSI solution (8.8 μL) for 30 min at 70 °C. All procedures were carried out in air. Finally, Au electrodes were evaporated as top electrodes [36]. Layered structures of the present photovoltaic cells are denoted as FTO/TiO<sub>2</sub>/MAPbI<sub>3</sub>/(DPPS)/Spiro-OMeTAD/Au, as shown in a schematic illustration of Figure 1.

The  $J$ - $V$  characteristics (Keysight B2901A, Keysight Technologies, Santa Rosa, CA, USA) of the photovoltaic cells were measured under illumination at  $100 \text{ mW cm}^{-2}$  by using an AM 1.5 solar simulator (San-ei Electric XES-301S, San-Ei Electric Co. Ltd., Osaka, Japan). The solar cells were illuminated through the side of the FTO substrates and the measurement area was  $0.090 \text{ cm}^2$ . The EQE of the cells was also investigated for the same devices (QE-R, Enli Technology, Enli Technology Co. Ltd., Kaohsiung, Taiwan). The microstructures of the perovskite layers were investigated using an X-ray diffractometer (D2 PHASER, Bruker, Billerica, MA, USA), an optical microscope (Eclipse E600, Nikon, Tokyo, Japan), and a scanning electron microscope (JSM-6010PLUS/LA, Jeol, Tokyo, Japan).

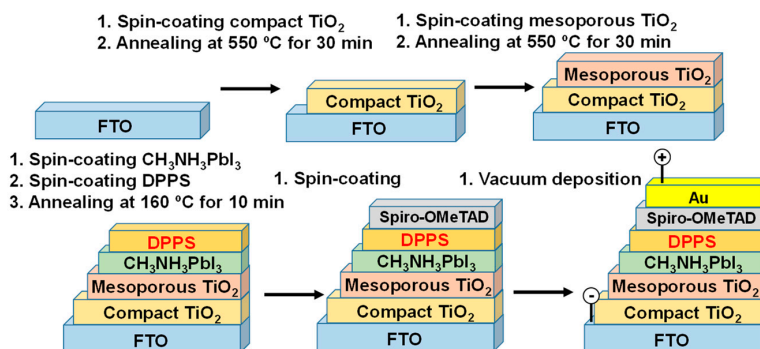


**Figure 1.** Schematic illustration of the fabrication process of the proposed photovoltaic devices.

### 3. Results and Discussion

$J$ - $V$  characteristics of the FTO/TiO<sub>2</sub>/MAPbI<sub>3</sub>/(DPPS)/Spiro-OMeTAD/Au photovoltaic cells under illumination are shown in Figure 2a. Measured photovoltaic parameters of the MAPbI<sub>3</sub>/(DPPS) cells are summarized in Table 1. EQE spectra of FTO/TiO<sub>2</sub>/MAPbI<sub>3</sub>/(DPPS)/Spiro-OMeTAD/Au cells are shown in Figure 2b. In Figure 2a, the MAPbI<sub>3</sub> cell provided the short circuit current density ( $J_{SC}$ ) of  $17.77 \text{ mA cm}^{-2}$ , the open circuit voltage ( $V_{OC}$ ) of  $0.833 \text{ V}$ , the fill factor ( $FF$ ) of  $0.349$ , and the conversion efficiency ( $\eta$ ) of  $5.16\%$ . The perovskite solar cells added with  $10 \text{ mg mL}^{-1}$  DPPS showed the highest conversion efficiency of  $8.27\%$  and highest average efficiency ( $\eta_{ave}$ ) of the four electrodes. In the devices with DPPS added, series resistance ( $R_s$ ) and shunt resistance ( $R_{sh}$ ) were improved, and the  $FF$  was improved. The DPPS addition decreased the  $J_{SC}$ , due to an increase in electric resistance by formation of the DPPS film. In Figure 2b, the standard device showed the highest EQE value, which agrees with the highest  $J_{SC}$  value in Figure 2a.

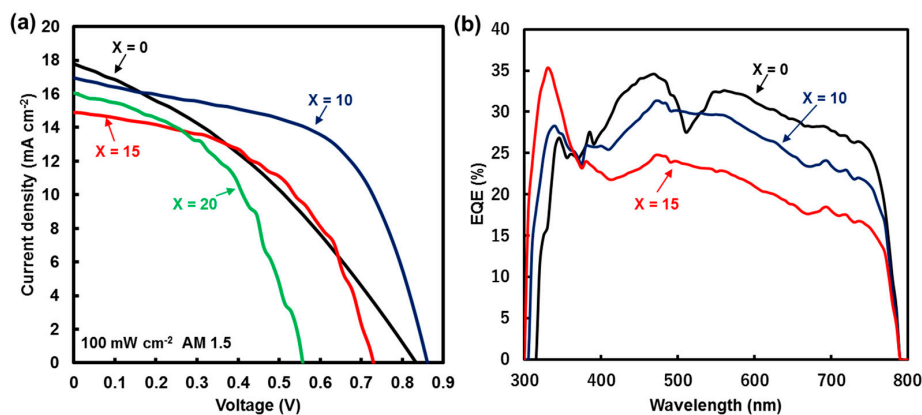


**Figure 2.** (a)  $J$ - $V$  characteristics and (b) External quantum efficiency (EQE) spectra of the CH<sub>3</sub>NH<sub>3</sub>PbI<sub>3</sub> (MAPbI<sub>3</sub>)/dipeptidylpeptidase (DPPS) ( $X \text{ mg mL}^{-1}$ ) cells.

**Table 1.** Measured photovoltaic parameters of MAPbI<sub>3</sub>/(DPPS) (*X* mg mL<sup>−1</sup>) perovskite solar cells.

| DPPS <i>X</i> (mg mL <sup>−1</sup> ) | <i>J</i> <sub>SC</sub> (mA cm <sup>−2</sup> ) | <i>V</i> <sub>OC</sub> (V) | <i>FF</i> | <i>η</i> (%) | <i>η</i> <sub>ave</sub> (%) | <i>R</i> <sub>s</sub> (Ω cm <sup>2</sup> ) | <i>R</i> <sub>sh</sub> (Ω cm <sup>2</sup> ) |
|--------------------------------------|---|----------------------------|-----------|--------------|-----------------------------|--|---|
| 0                                    | 17.77   | 0.833                      | 0.349     | 5.16         | 2.07                        | 28.0                                       | 105   |
| 10                                   | 16.97   | 0.861                      | 0.566     | 8.27         | 4.33                        | 9.15                                       | 245   |
| 15                                   | 14.88   | 0.729                      | 0.511     | 5.55         | 2.58                        | 9.91                                       | 314   |
| 20                                   | 16.06   | 0.558                      | 0.487     | 4.36         | 3.63                        | 9.95                                       | 186   |

Optical microscope images of MAPbI<sub>3</sub>/(DPPS) (*X* mg mL<sup>−1</sup>) perovskite solar cells are shown in Figure 3a–d. Devices with added DPPS had smaller sizes of perovskite crystals, and density of grain distribution was improved compared with the standard device. We suggest that the charge recombination was suppressed by the improvement in density. Therefore, the conversion efficiency was improved in the device to which 10 mg mL<sup>−1</sup> DPPS was added.

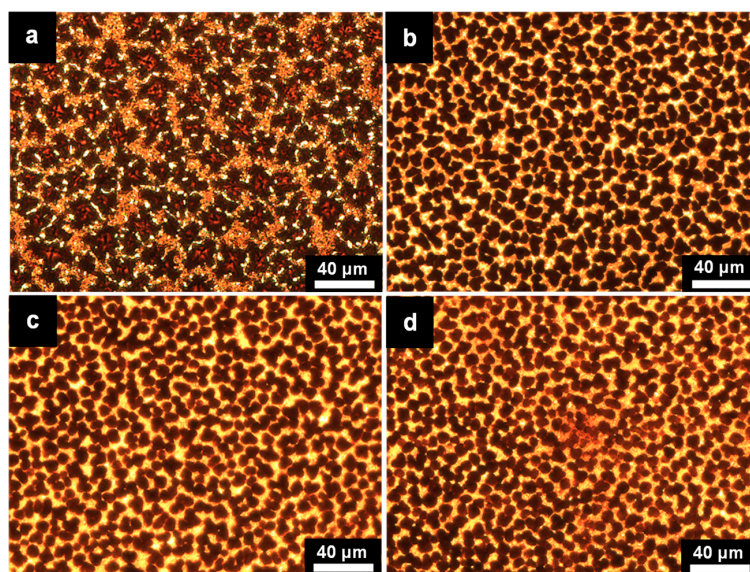
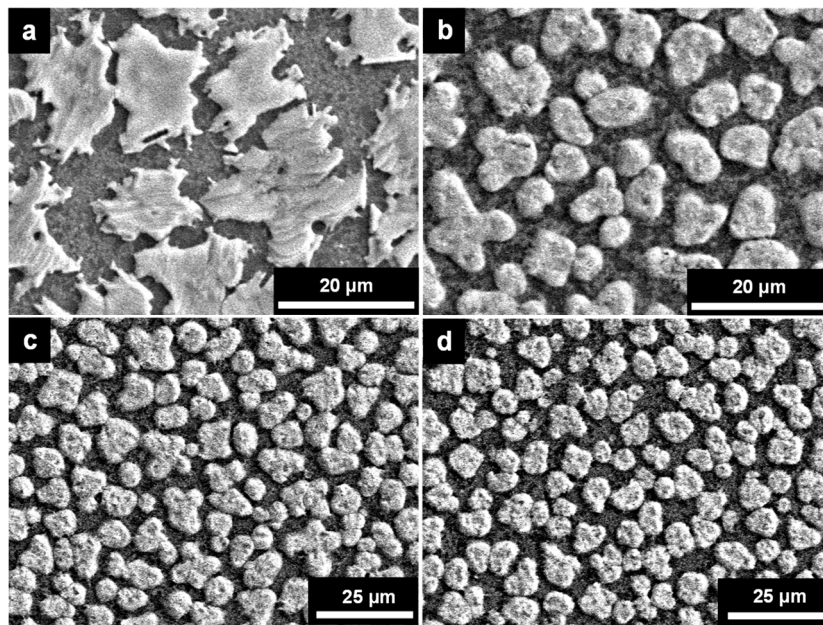
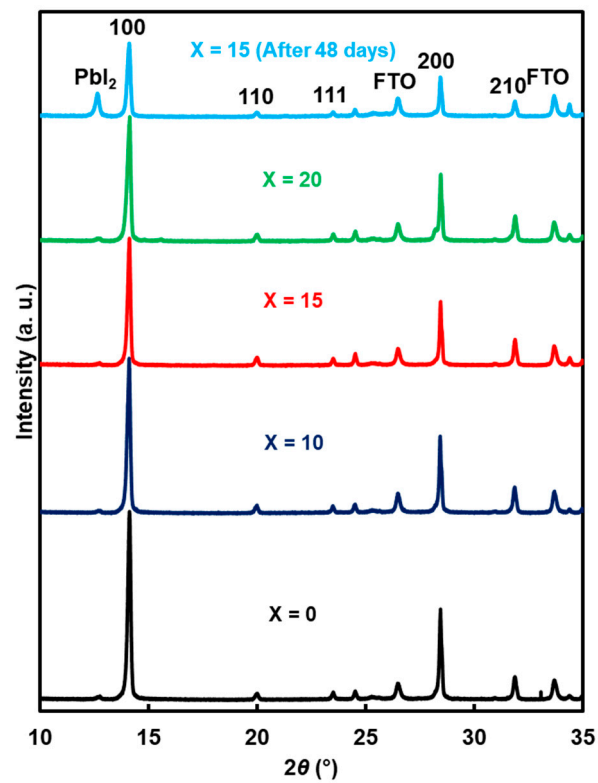
**Figure 3.** Optical microscope images of the MAPbI<sub>3</sub>/(DPPS) perovskite solar cells. The concentration of DPPS are (a) 0 mg mL<sup>−1</sup>, (b) 10 mg mL<sup>−1</sup>, (c) 15 mg mL<sup>−1</sup>, and (d) 20 mg mL<sup>−1</sup>.

Figure 4a–d are SEM images of MAPbI<sub>3</sub>/(DPPS) (*X* mg mL<sup>−1</sup>) perovskite solar cells. In the devices to which DPPS was added, the morphology of the perovskite crystal was drastically changed, and the interval of the crystal grains decreased compared with the standard device. We suggest that DPPS affected the crystal growth of the perovskite layer and the surface coverage was improved. The perovskite film also exists in the dark areas of the SEM images and bright areas of the optical microscope images. The crystal grains observed in the SEM images were larger perovskite grains on the perovskite film. Therefore, the TiO<sub>2</sub> layers was not exposed to the spiro-OMeTAD.

XRD patterns of MAPbI<sub>3</sub>/(DPPS) (*X* mg mL<sup>−1</sup>) photovoltaic cells are shown in Figure 5. Measured XRD parameters of the MAPbI<sub>3</sub>/(DPPS) (*X* mg mL<sup>−1</sup>) cells are summarized in Table 2. As shown in Figure 5, the DPPS-added devices show almost the same peaks compared with those of the standard device, which indicates that the perovskite structure is preserved. When the devices were measured after about seven weeks, a peak of PbI<sub>2</sub> was detected. Crystallite sizes of the perovskite for the cell with 15 mg mL<sup>−1</sup> DPPS decreased after 48 days. This is assumed to be due to a part of the perovskite crystals turning into a PbI<sub>2</sub> crystal by desorption of CH<sub>3</sub>NH<sub>2</sub> and HI from the CH<sub>3</sub>NH<sub>3</sub>PbI<sub>3</sub>, and the PbI<sub>2</sub> crystal precipitating on the surface of the perovskite layer, thereby decreasing the crystallite sizes. This change in crystallite size has little relation to the change in conversion efficiency. Since the PbI<sub>2</sub> is a *p*-type semiconductor, the thin PbI<sub>2</sub> precipitation on the surface of the perovskite layer promotes hole transport and also functions as an electron blocking layer. Therefore, the charge recombination was suppressed, and the conversion efficiency was improved.



**Figure 4.** SEM images of the MAPbI<sub>3</sub>/(DPPS) perovskite solar cells. The concentration of DPPS are (a) 0 mg mL<sup>-1</sup>, (b) 10 mg mL<sup>-1</sup>, (c) 15 mg mL<sup>-1</sup>, and (d) 20 mg mL<sup>-1</sup>.



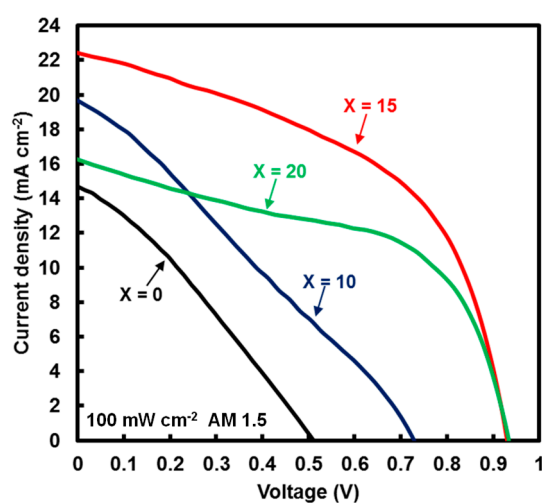
**Figure 5.** XRD patterns of the MAPbI<sub>3</sub>/(DPPS) (X mg mL<sup>-1</sup>) perovskite solar cells.

**Table 2.** XRD parameters of 100 of the MAPbI<sub>3</sub>/(DPPS) (X mg mL<sup>-1</sup>) perovskite solar cells.

| DPPS X (mg mL <sup>-1</sup> ) | Lattice Constant (Å) | Crystallite Size (Å) |
|-------------------------------|----------------------|----------------------|
| 0                             | 6.268                | 536                  |
| 10                            | 6.275                | 510                  |
| 15                            | 6.271                | 537                  |
| 20                            | 6.263                | 464                  |
| 15 *                          | 6.273                | 467                  |

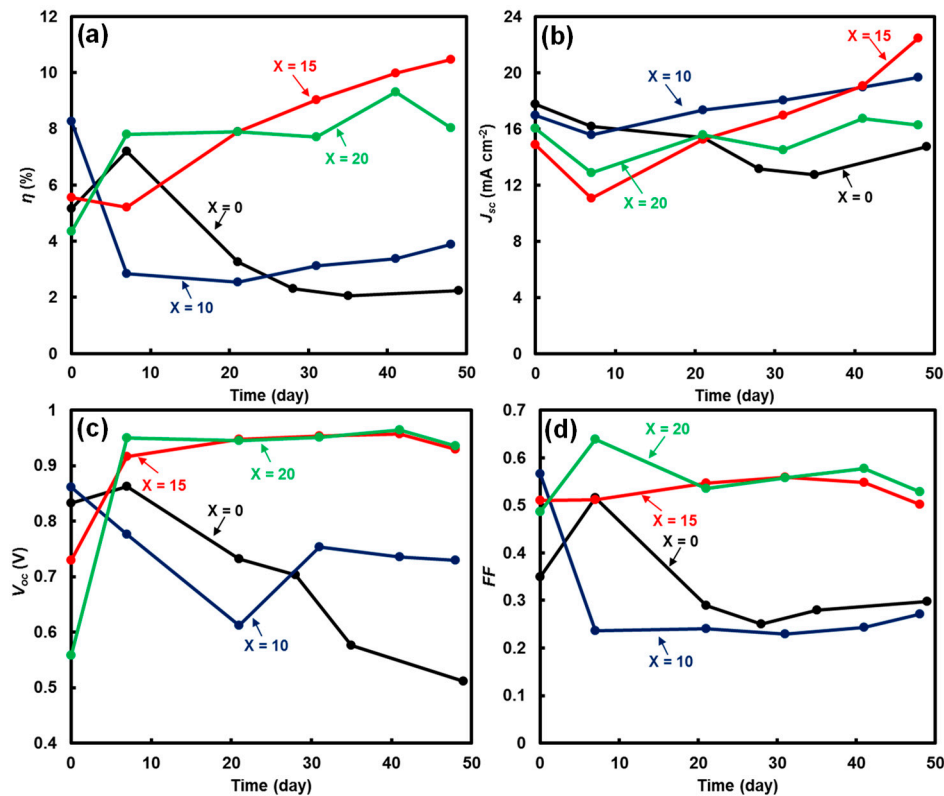
\* Measurements of the device after 48 days.

Figure 6 is the  $J$ - $V$  characteristics of the FTO/TiO<sub>2</sub>/MAPbI<sub>3</sub>/(DPPS)/Spiro-OMeTAD/Au photovoltaic cells after about seven weeks (48 days), and the measured photovoltaic parameters are also summarized in Table 3. As shown in Figure 6, while the conversion efficiency was lowered in the standard device after about seven weeks, the conversion efficiency was improved in the device added with 15 mg mL<sup>-1</sup> DPPS. Especially remarkable improvement of  $J_{SC}$  and  $V_{OC}$  was observed for the device to which 15 mg mL<sup>-1</sup> DPPS was added. As listed in Table 1, the device containing 10 mg mL<sup>-1</sup> DPPS provided the highest conversion efficiency, which was due to the thin film thickness and low electrical resistance. However, an increasing amount of the PbI<sub>2</sub> crystals were formed and the  $\eta$  values decreased after 48 days, which was due to the lower surface coverage of DPPS. On the other hand, the conversion efficiency of the device with 15 mg mL<sup>-1</sup> DPPS was lower than that of the standard cell, because of the increased electrical resistance. However, the conversion efficiency improved after 48 days. Since the perovskite layer can be sufficiently covered by the DPPS, decomposition of the perovskite crystals was suppressed, and the  $p$ -type semiconducting characteristics of DPPS and PbI<sub>2</sub> improved the conversion efficiency.

**Figure 6.**  $J$ - $V$  characteristics of the MAPbI<sub>3</sub>/(DPPS) (X mg mL<sup>-1</sup>) perovskite solar cells. The standard system is the device after 49 days, and the system added with DPPS is the device after 48 days.**Table 3.** Measured photovoltaic parameters of the MAPbI<sub>3</sub>/(DPPS) (X mg mL<sup>-1</sup>) perovskite solar cells. The standard device is after 49 days and the device added with DPPS is after 48 days.

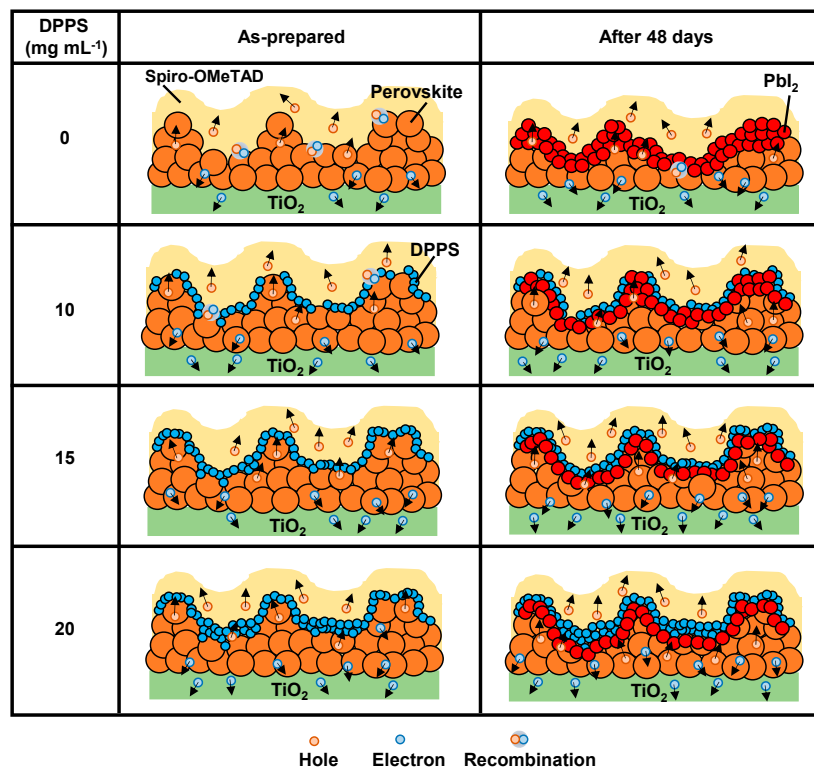
| DPPS X (mg mL <sup>-1</sup> ) | $J_{SC}$ (mA cm <sup>-2</sup> ) | $V_{OC}$ (V) | FF    | $\eta$ (%) | $\eta_{ave}$ (%) | $R_s$ ( $\Omega$ cm <sup>2</sup> ) | $R_{sh}$ ( $\Omega$ cm <sup>2</sup> ) |
|-------------------------------|---------------------------------|--------------|-------|------------|------------------|------------------------------------|---------------------------------------|
| 0                             | 14.72                           | 0.512        | 0.298 | 2.24       | 1.97             | 25.4                               | 67.9                                  |
| 10                            | 19.68                           | 0.729        | 0.271 | 3.90       | 3.57             | 18.5                               | 61.9                                  |
| 15                            | 22.45                           | 0.929        | 0.502 | 10.48      | 8.28             | 7.17                               | 143                                   |
| 20                            | 16.26                           | 0.935        | 0.528 | 8.03       | 6.24             | 7.59                               | 214                                   |

Figure 7 shows results of the stability measurements of the presented cells up to about 7 weeks. Photovoltaic parameters are also summarized in Table 3. For the DPPS-added devices, the  $J_{SC}$  values increased, which is abnormal behavior for the perovskite photovoltaic devices. Improvement or stabilization of the parameters were observed for the devices to which DPPS of  $15 \text{ mg mL}^{-1}$  or more was added.



**Figure 7.** Stability measurements of the  $\text{MAPbI}_3/(\text{DPPS})$  ( $X \text{ mg mL}^{-1}$ ) perovskite solar cells. (a–d) respectively, show photoelectric conversion efficiency ( $\eta$ ), short circuit current density ( $J_{sc}$ ), open circuit voltage ( $V_{oc}$ ) and fill factor ( $FF$ ).

Figure 8 shows schematic models of microstructure, carrier dynamics, and stability of the proposed devices. The standard device without DPPS has defect structures, which cause charge recombination and charge trapping. Although  $\text{PbI}_2$  precipitation might suppress charge recombination for the standard device after 48 days, the conversion efficiency decreased due to the large amount of precipitated  $\text{PbI}_2$ . For the devices with DPPS, defects of the perovskite layers were reduced by the DPPS layer and charge recombination was suppressed. For the devices with DPPS, after 48 days the formed  $\text{PbI}_2$  crystals and the DPPS layer acted as an electron blocking layer that promoted charge transfer. As a result, the stability was good and the conversion efficiency improved. For the device with  $10 \text{ mg mL}^{-1}$  DPPS, more  $\text{PbI}_2$  crystals formed over time and the  $\eta$  values decreased after 48 days. This was due to the lower surface coverage of DPPS, which is sensitive to the influence of oxygen and moisture in the air. For devices with  $15$  and  $20 \text{ mg mL}^{-1}$  DPPS, the stability improved because the DPPS layer sufficiently covered the perovskite layer. However, for the device with  $20 \text{ mg mL}^{-1}$  DPPS, the electrical resistance increased as the thickness of the DPPS layer increased, and the conversion efficiency was lower than that of the device with  $15 \text{ mg mL}^{-1}$  DPPS.



**Figure 8.** Schematic illustration of the microstructure, carrier dynamics and stability models for perovskite solar cells with different DPPS concentration.

#### 4. Conclusions

Perovskite-based solar cells were fabricated by a spin-coating method, and the effects of DPPS addition on top of the perovskite layers on the photovoltaic properties were investigated. From the results of  $J-V$  characteristics,  $FF$  was improved by adding DPPS. For the device with  $15 \text{ mg mL}^{-1}$  DPPS, the  $J_{SC}$  and  $V_{OC}$  increased, and the photoelectric conversion efficiency was remarkably improved, even after 48 days. Microstructure analysis by optical microscopy and SEM indicated that the morphology of the perovskite crystals was drastically changed, and the grain density was improved. X-ray diffraction analysis showed that the crystal structure did not change, even when DPPS was added to the standard system. The photoelectric conversion efficiency of the device with  $15 \text{ mg mL}^{-1}$  DPPS device was improved even after 48 days, which indicates that the charge transfer was accelerated by the  $\text{PbI}_2$  layer, and that the DPPS layer acted as an electron blocking layer.

**Author Contributions:** Conceptualization, M.T. and T.O.; Methodology, M.T.; Validation, A.S.; Formal Analysis, M.T.; Investigation, M.T.; Resources, S.F., S.M. and M.O.; Data Curation, M.T. and T.O.; Writing-Original Draft Preparation, M.T.; Writing-Review & Editing, T.O., A.S., S.F., S.M. and M.O.; Visualization, M.T. and T.O.; Supervision, T.O. and A.S.; Project Administration, T.O.; Funding Acquisition, T.O.

**Funding:** This research was funded by the Super Cluster Program of the Japan Science and Technology Agency (JST).

**Conflicts of Interest:** The authors declare no conflict of interest.

#### References

- Pan, Y.Y.; Su, Y.H.; Hsu, C.H.; Huang, L.W.; Dou, K.P.; Kaun, C.C. First-principles study on electronic structures of  $\text{FAPbX}_3$  ( $X = \text{Cl, Br, I}$ ) hybrid perovskites. *J. Adv. Nanomater.* **2016**, *1*, 33–38. [[CrossRef](#)]
- Wang, J.F.; Zhu, L.; Zhao, B.G.; Zhao, Y.L.; Song, J.; Gu, X.Q.; Qiang, Y.H. Surface engineering of perovskite films for efficient solar cells. *Sci. Rep.* **2017**, *7*, 14478. [[CrossRef](#)] [[PubMed](#)]

3. Xu, W.; Zheng, L.; Zhang, X.; Cao, Y.; Meng, T.; Wu, D.; Liu, L.; Hu, W.; Gong, X. Efficient perovskite solar cells fabricated by Co partially substituted hybrid perovskite. *Adv. Energy Mater.* **2018**, *10*, 1703178. [[CrossRef](#)]
4. Li, X.; Zhang, W.; Wang, Y.C.; Zhang, W.; Wang, H.Q.; Fang, J. In-situ cross-linking strategy for efficient and operationally stable methylammonium lead iodide solar cells. *Nat. Commun.* **2018**, *9*, 3806. [[CrossRef](#)] [[PubMed](#)]
5. Cortecchia, D.; Dewi, H.A.; Yin, J.; Bruno, A.; Chen, S.; Baikie, T.; Boix, P.P.; Gratzel, M.; Mhaisalkar, S.; Soci, C.; et al. Lead-free MA<sub>2</sub>CuCl<sub>x</sub>Br<sub>4-x</sub> hybrid perovskites. *Inorg. Chem.* **2016**, *55*, 1044–1052. [[CrossRef](#)] [[PubMed](#)]
6. Gedamu, D.; Asuo, I.M.; Benetti, D.; Basti, M.; Ka, I.; Cloutier, S.G.; Rosei, F.; Nechache, R. Solvent-antisolvent ambient processed large grain size perovskite thin films for high-performance solar cells. *Sci. Rep.* **2018**, *8*, 12885. [[CrossRef](#)] [[PubMed](#)]
7. Klug, M.T.; Osherov, A.; Haghghirad, A.A.; Stranks, S.D.; Brown, P.R.; Bai, S.; Wang, J.T.W.; Dang, X.; Bulovic, V.; Snaith, H.J.; et al. Tailoring metal halide perovskites through metal substitution: influence on photovoltaic and material properties. *Energy Environ. Sci.* **2017**, *10*, 236–246. [[CrossRef](#)]
8. Yang, W.S.; Park, B.W.; Jung, E.H.; Jeon, N.J.; Kim, Y.C.; Lee, D.U.; Shin, S.S.; Seo, J.; Kim, E.K.; Noh, J.H.; et al. Iodide management in formamidinium-lead-halide-based perovskite layers for efficient solar cells. *Science* **2017**, *356*, 1376–1379. [[CrossRef](#)]
9. Wang, F.; Bai, S.; Tress, W.; Hagfeldt, A.; Gao, F. Defects engineering for high-performance perovskite solar cells. *NPJ Flex. Electron.* **2018**, *2*, 22. [[CrossRef](#)]
10. Ng, C.H.; Ripolles, T.S.; Hamada, K.; Teo, S.H.; Lim, H.N.; Bisquert, J.; Hayase, S. Tunable open circuit voltage by engineering inorganic cesium lead bromide/iodide perovskite solar cells. *Sci. Rep.* **2018**, *8*, 2482. [[CrossRef](#)]
11. Li, N.; Zhu, Z.; Chueh, C.C.; Liu, H.; Peng, B.; Petrone, A.; Li, X.; Wang, L.; Jen, A.K.Y. Mixed cation FA<sub>x</sub>PEA<sub>1-x</sub>PbI<sub>3</sub> with enhanced phase and ambient stability toward high-performance perovskite solar cells. *Adv. Energy Mater.* **2017**, *7*, 1601307. [[CrossRef](#)]
12. Zhang, X.; Yin, J.; Nie, Z.; Zhang, Q.; Sui, N.; Chen, B.; Zhang, Y.; Qu, K.; Zhao, J.; Zhou, H. Lead-free and amorphous organic-inorganic hybrid materials for photovoltaic applications: Mesoscopic CH<sub>3</sub>NH<sub>3</sub>MnI<sub>3</sub>/TiO<sub>2</sub> heterojunction. *RSC Adv.* **2017**, *7*, 37419–37425. [[CrossRef](#)]
13. Mali, S.S.; Shim, C.S.; Hong, C.K. Highly stable and efficient solid-state solar cells based on methylammonium lead bromide (CH<sub>3</sub>NH<sub>3</sub>PbBr<sub>3</sub>) perovskite quantum dots. *NPG Asia Mater.* **2015**, *7*, e208. [[CrossRef](#)]
14. Chen, H.W.; Huang, T.Y.; Chang, T.H.; Sanehira, Y.; Kung, C.W.; Chu, C.W.; Ikegami, M.; Miyasaka, T.; Ho, K.C. Efficiency enhancement of hybrid perovskite solar cells with MEH-PPV hole transporting layers. *Sci. Rep.* **2016**, *6*, 34319. [[CrossRef](#)] [[PubMed](#)]
15. Zuo, L.; Guo, H.; deQuilettes, D.W.; Jariwala, S.; Marco, N.D.; Dong, S.; De Block, R.; Ginger, D.S.; Dunn, B.; Wang, M.; et al. Polymer-modified halide perovskite films for efficient and stable planar heterojunction solar cells. *Sci. Adv.* **2017**, *3*, e1700106. [[CrossRef](#)] [[PubMed](#)]
16. Zhang, S.; Lu, Y.; Lin, B.; Zhu, Y.; Zhang, K.; Yuan, N.Y.; Ding, J.N.; Fang, B. PVDF-HFP additive for visible-light-semi-transparent perovskite films yielding enhanced photovoltaic performance. *Sol. Energy Mater. Sol. Cells* **2017**, *170*, 178–186. [[CrossRef](#)]
17. Chen, Z.; Dong, Q.; Liu, Y.; Bao, C.; Fang, Y.; Lin, Y.; Tang, S.; Wang, Q.; Xiao, X.; Bai, Y.; et al. Thin single crystal perovskite solar cells to harvest below-bandgap light absorption. *Nat. Commun.* **2017**, *8*, 1890. [[CrossRef](#)]
18. Zhang, H.; Shi, J.; Zhu, L.; Luo, Y.; Li, D.; Wu, H.; Meng, Q. Polystyrene stabilized perovskite component, grain and microstructure for improved efficiency and stability of planar solar cells. *Nano Energy* **2018**, *43*, 383–392. [[CrossRef](#)]
19. Tavakoli, M.M.; Tavakoli, R.; Prochowicz, D.; Yadav, P.; Saliba, M. Surface modification of a hole transporting layer for an efficient perovskite solar cell with an enhanced fill factor and stability. *Mol. Syst. Des. Eng.* **2018**, *3*, 717–722. [[CrossRef](#)]
20. Dubey, A.; Adhikari, N.; Mabrouk, S.; Wu, F.; Chen, K.; Yang, S.; Qiao, Q. A strategic review on processing routes towards highly efficient perovskite solar cells. *J. Mater. Chem. A* **2018**, *6*, 2406–2431. [[CrossRef](#)]
21. Wang, D.; Chan, K.H.; Elumalai, N.K.; Mahmud, M.A.; Upama, M.B.; Uddin, A.; Pillai, S. Interfacial engineering of hole transport layers with metal and dielectric nanoparticles for efficient perovskite solar cells. *Phys. Chem. Chem. Phys.* **2017**, *19*, 25016–25024. [[CrossRef](#)] [[PubMed](#)]

22. Mabrouk, S.; Zhang, M.; Wang, Z.; Liang, M.; Bahrami, B.; Wu, Y.; Wu, J.; Qiao, Q.; Yang, S. Dithieno[3,2-b:2',3'-d] pyrrole-based hole transport materials for perovskite solar cells with efficiencies over 18%. *J. Mater. Chem. A* **2018**, *6*, 7950–7958. [[CrossRef](#)]
23. Gaml, E.A.; Dubey, A.; Reza, K.M.; Hasan, M.N.; Adhikari, N.; Elbohy, H.; Bahrami, B.; Zeyada, H.; Yang, S.; Qiao, Q. Alternative benzodithiophene (BDT) based polymeric hole transport layer for efficient perovskite solar cells. *Sol. Energy Mater. Sol. Cells* **2017**, *168*, 8–13. [[CrossRef](#)]
24. Bi, D.; Yi, C.; Luo, J.; Decoppet, J.D.; Zhang, F.; Zakeeruddin, S.M.; Li, X.; Hagfeldt, A.; Gratzel, M. Polymer-templated nucleation and crystal growth of perovskite films for solar cells with efficiency greater than 21%. *Nat. Energy* **2016**, *1*, 16142. [[CrossRef](#)]
25. Wang, F.; Endo, M.; Mouri, S.; Miyauchi, Y.; Ohno, Y.; Wakamiya, A.; Murata, Y.; Matsuda, K. Highly stable perovskite solar cells with an all-carbon hole transport layer. *Nanoscale* **2016**, *8*, 11882–11888. [[CrossRef](#)] [[PubMed](#)]
26. Stranks, S.D.; Eperon, G.E.; Grancini, G.; Menelaou, C.; Alcocer, M.J.P.; Leijtens, T.; Herz, L.M.; Petrozza, A.; Snaith, H.J. Electron-hole diffusion lengths exceeding 1 micrometer in an organometal trihalide perovskite absorber. *Science* **2013**, *342*, 341–344. [[CrossRef](#)]
27. Taguchi, M.; Suzuki, A.; Tanaka, H.; Oku, T. Fabrication and characterization of perovskite solar cells added with MnCl<sub>2</sub>, YCl<sub>3</sub> or poly(methyl methacrylate). *AIP Conf. Proc.* **2018**, *1929*, 020012.
28. Wang, F.; Shimazaki, A.; Yang, F.; Kanahashi, K.; Matsuki, K.; Miyauchi, Y.; Takenobu, T.; Wakamiya, A.; Murata, Y.; Matsuda, K. Highly efficient and stable perovskite solar cells by interfacial engineering using solution-processed polymer layer. *J. Phys. Chem. C* **2017**, *121*, 1562–1568. [[CrossRef](#)]
29. Oku, T.; Nakagawa, J.; Iwase, M.; Kawashima, A.; Yoshida, K.; Suzuki, A.; Akiyama, T.; Tokumitsu, K.; Yamada, M.; Nakamura, M. Microstructures and photovoltaic properties of polysilane-based solar cells. *Jpn. J. Appl. Phys.* **2013**, *52*, 04CR07. [[CrossRef](#)]
30. Nakagawa, J.; Oku, T.; Suzuki, A.; Akiyama, T.; Yamada, M.; Fukunishi, S.; Kohno, K. Effects of PBr<sub>3</sub> addition to polysilane thin films on structures and photovoltaic properties. *Green Sustain. Chem.* **2017**, *7*, 20–34. [[CrossRef](#)]
31. Oku, T.; Hibi, N.; Suzuki, A.; Akiyama, T.; Yamada, M.; Fukunishi, S.; Kohno, K. Effects of triphenylborane addition to decaphenylcyclopentasilane thin films. *Jpn. Soc. Appl. Phys. Conf. Proc.* **2015**, *3*, 011404.
32. Shirahata, Y.; Yamamoto, Y.; Suzuki, A.; Oku, T.; Fukunishi, S.; Kohno, K. Effects of polysilane-doped spiro-OMeTAD hole transport layers on photovoltaic properties. *Phys. Status Solidi A* **2017**, *214*, 1600591. [[CrossRef](#)]
33. Shirahata, Y.; Oku, T.; Fukunishi, S.; Kohno, K. Fabrication of perovskite-type photovoltaic devices with polysilane hole transport layers. *Mater. Sci. Appl.* **2017**, *8*, 209–222. [[CrossRef](#)]
34. Oku, T.; Nomura, J.; Suzuki, A.; Tanaka, H.; Fukunishi, S.; Minami, S.; Tsukada, S. Fabrication and characterization of CH<sub>3</sub>NH<sub>3</sub>PbI<sub>3</sub> perovskite solar cells added with polysilanes. *Int. J. Photoenergy* **2018**, *2018*, 8654963. [[CrossRef](#)]
35. Oku, T.; Zushi, M.; Imanishi, Y.; Suzuki, A.; Suzuki, K. Microstructures and photovoltaic properties of perovskite-type CH<sub>3</sub>NH<sub>3</sub>PbI<sub>3</sub> compounds. *Appl. Phys. Express* **2014**, *7*, 121601. [[CrossRef](#)]
36. Oku, T.; Suzuki, K.; Suzuki, A. Effects of chlorine addition to perovskite-type CH<sub>3</sub>NH<sub>3</sub>PbI<sub>3</sub> photovoltaic devices. *J. Ceram. Soc. Jpn.* **2016**, *124*, 234–238. [[CrossRef](#)]
37. Oku, T.; Ohishi, Y.; Suzuki, A.; Miyazawa, Y. Effects of NH<sub>4</sub>Cl addition to perovskite CH<sub>3</sub>NH<sub>3</sub>PbI<sub>3</sub> photovoltaic devices. *J. Ceram. Soc. Jpn.* **2017**, *125*, 303–307. [[CrossRef](#)]
38. Li, Y.; Sun, W.; Yan, W.; Ye, S.; Rao, H.; Peng, H.; Zhao, Z.; Bian, Z.; Liu, Z.; Zhou, H.; et al. 50% Sn-based planar perovskite solar cell with power conversion efficiency up to 13.6%. *Adv. Energy Mater.* **2016**, *6*, 1601353. [[CrossRef](#)]
39. Ueoka, N.; Oku, T.; Ohishi, Y.; Tanaka, H.; Suzuki, A. Effects of excess PbI<sub>2</sub> addition to CH<sub>3</sub>NH<sub>3</sub>PbI<sub>3-x</sub>Cl<sub>x</sub> perovskite solar cells. *Chem. Lett.* **2018**, *47*, 528–531. [[CrossRef](#)]
40. Oku, T.; Ohishi, Y.; Ueoka, N. Highly (100)-oriented CH<sub>3</sub>NH<sub>3</sub>PbI<sub>3</sub> (Cl) perovskite solar cells prepared with NH<sub>4</sub>Cl using an air blow method. *RSC Adv.* **2018**, *8*, 10389–10395. [[CrossRef](#)]
41. Oku, T.; Ohishi, Y. Effects of annealing on CH<sub>3</sub>NH<sub>3</sub>PbI<sub>3</sub> (Cl) perovskite photovoltaic devices. *J. Ceram. Soc. Jpn.* **2018**, *126*, 56–60. [[CrossRef](#)]

